# Influence of Polarization State on Ultrafast Laser-Induced Bulk Nanostructuring

Anton Rudenko, Jean-Philippe Colombier, and Tatiana E. Itina

*Univ Lyon, UJM Saint-Etienne, Laboratoire Hubert Curien, CNRS UMR 5516, F-42000, Saint-Etienne, France*
*E-mail: anton.rudenko@univ.st-etienne.fr*

Using an electromagnetic approach based on three-dimensional Maxwell's equations coupled with electron density equation, we investigate femtosecond laser interaction with fused silica containing randomly distributed inhomogeneities. By irradiating with linearly, radially, azimuthally, circularly and mixed polarized beams, we visualize and analyze the resulting electron density distributions in glass. The numerical calculations demonstrate the local material excitation to the polarization state of light and underline the nanostructure orientation perpendicular to the local laser polarization. The advantages of using azimuthal- and radial-variant polarizations to produce the nanogratings with desirable characteristics are discussed. Circularly polarized beams are shown to be, on the contrary, beneficial to prevent the nanostructure self-organization.
DOI: 10.2961/jlmn.2016.03.0004
**Keywords:** self-organized nanogratings, femtosecond laser irradiation, polarization, nanostructuring, Maxwell's equations, FDTD, electron density evolution, laser-induced inhomogeneities.

## 1. Introduction

Femtosecond laser processing enables imprinting nanoscale periodic structures on the surface of metals [1-4], semiconductors [5-7] and dielectrics [8-10], inside glass materials such as fused silica [11-15], and several indirect bandgap semiconductors [16-18]. The orientation of the nanostructures depends on the local laser polarization. For instance, it is possible to rotate the nanoplanes imprinted in fused silica bulk in space [14] and to inscribe the nanogratings and the nanoripples of the designable spatial structure [19]. Many experimental works were devoted to reveal nanostructures created by radial and azimuthal polarizations [1, 3, 5-6, 13, 15, 20], circular polarization [19, 21-22], and even spiral polarization [4, 7, 23]. Such nanostructures can find a wide range of applications in the fabrication of polarization-sensitive devices [24-25] and computer-generated holography [26], in five-dimensional optical data storage [27], material security marking and fighting against counterfeiting [28], fabrication of nanofluidics channels for biomedicine and DNA molecular analysis [29], and in the synthesis of chiral materials [13].

Particularly, the advantage of using complex cylindrical polarizations was discussed. Firstly, both radial and azimuthal polarization beams are rotationally symmetric and isotropic. Secondly, they are expected to increase processing efficiency, quality and speed of the femtosecond laser processing [1, 22, 30-31]. Thus, radial polarized fields are better than linear scalar fields for excitation of surface plasmon polaritons [32-34], detection, manipulating, optical trapping and reshaping of nanoparticles [35-38], quantum information processing [39-40], and sub-wavelength nanostructuring [3-4, 7, 19, 23].

Recent experimental approaches offer a possibility not only to create vector fields with azimuthally-dependent polarization [4, 6-7, 19-20], but also to apply arbitrarily patterned vector optical fields varying spatial arrangement and distributions of states of polarization by using spatial light modulators [28, 41-43]. Here, we propose that such a technique could be useful not only for high-speed fabrication of periodic nanostructures with femtosecond laser processing, but also for improving and controlling the characteristics of the nanostructures. Particularly, using the vector optical fields with combined azimuthal- and radial-variant polarization [39, 43-47] might serve to tune the period and the thickness of the nanostructures.

Ripple formation and distortions might be on the contrary undesirable for accurate femtosecond material processing, laser drilling and laser lithography [12, 48]. Circularly polarized beams were shown to produce no gratings but random nanodot deposits [49-54] and much less likely to undergo multiple filamentation than linearly polarized beams [55-56] because the input circular polarization state does not induce a preferred direction in the transverse plane. Therefore, they are advantageous to prevent the nanostructure organization on the surface [57-58] and in bulk of dielectrics [12, 21, 54, 59-60]. To determine more precisely the mechanisms taking place during ultrashort laser irradiation, we investigate numerically laser-matter interaction with circularly polarized beams.

The mechanism of the nanostructure formation is still under the debate [3, 7-8, 11, 61-68]. Previously, numerical approaches based on Maxwell's equations were developed to study the electromagnetic interaction of ultrashort laser irradiation with a rough surface [62, 69-71]. It was suggested that the interference patterns left by the inhomogeneous absorption of linear polarized laser radiation below a

rough surface corresponded to the localized surface ripples which could be organized within single laser shot [62]. The method was further expanded to take into account the interpulse feedback mechanisms [69, 71-72]. Moreover, Maxwell's equations were coupled with electron density equation to investigate the dynamics of the interaction with randomly distributed inhomogeneities in fused silica glass to explain the self-organization of nanogratings which require multiple pulse evolution related to multiphoton ionization memory feedback [64, 73].

We have recently developed a nonlinear electromagnetic approach to describe the mechanism of the nanostructure formation from random inhomogeneities by linearly polarized ultrashort laser pulses [73]. In this work, we provide new insights into the phenomena by calculating and visualizing the three-dimensional electron density profiles, and by considering the role of different laser polarizations in the formation of volume nanogratings. In particular, we numerically investigate the nanostructuring by radial, azimuthal and mixed polarizations and compare the results of the calculations with available experimental data. We suggest that radial-variant polarization discussed in a few recent articles [39, 44-47] might be advantageous in femtosecond laser nanostructuring and confirm it by calculating electron density profiles inscribed by the radial-variant polarization and comparing with the ones of the azimuthal-variant polarization. Results of numerical calculations reveal, however, that no nanogratings are formed by applying a circular polarization. We show that random nanodots observed in experiments with circular polarization [21, 49-54] are attributed to non-organized energy distribution in our calculation results. In addition, electron density profile induced by ultrashort laser irradiation with circular polarization is shown to be quasi-symmetrical even in the presence of laser-induced inhomogeneities in contrast to the electron density profile induced by linear polarization irradiation.

## 2. Numerical model

### 2.1 Electrodynamics

To investigate the effects of laser polarization on laser-induced nanostructuring, the finite-difference time-domain (FDTD) approach is applied for nonlinear and disperse media, where Maxwell's equations are written as:

$$\begin{cases} \dfrac{\partial}{\partial t}\vec{D} = \nabla \times \vec{H} - \vec{J_D} - \vec{J_{Kerr}} - \vec{J_{pi}} \\ \dfrac{\partial}{\partial t}\vec{H} = -\dfrac{\nabla \times \vec{E}}{\mu_0}, \end{cases} \quad (1)$$

where $\vec{D}$ is the displacement field, $\vec{E}$ is the electric field, $\vec{H}$ is the magnetic field, $\vec{J_D}$ is current derived from the Drude model for the dispersive media; $\vec{J_{Kerr}}$ is Kerr polarization current; and $\vec{J_{pi}}$ is the multiphoton ionization term.

For dielectric materials, such as fused silica, the heating of the conduction band electrons is modeled by Drude model with time-dependent carrier density as follows:

$$\frac{\partial}{\partial t}\vec{J_D} = -\frac{\vec{J_D}}{\tau_c} + \frac{e^2 n_e}{m_e}\vec{E}, \quad (2)$$

where $e$ is the elementary charge; $m_e$ is the mass of an electron; $n_e$ is the carrier electron density and $\tau_c = 0.5$ fs is the electron collision time reported in Ref. 74.

In addition, nonlinearity of the third order is included, which describes Kerr effect, as follows:

$$\vec{J_{Kerr}} = \varepsilon_0 \chi_3 \frac{\partial}{\partial t}\left(\left|\vec{E}\right|^2 \vec{E}\right), \quad (3)$$

where the third-order susceptibility is $\chi_3 = 2 \cdot 10^{-22}$ (m/V)$^2$ [75].

We consider a complete Keldysh ionization rate $w_{pi}(I)$ [76], including multiphoton and tunneling ionization, for which the corresponding current is written as:

$$\vec{J_{pi}} = E_g \frac{w_{pi}\vec{E}}{\left|\vec{E}\right|^2}\frac{n_a - n_e}{n_a}. \quad (4)$$

Here $E_g = 9$ eV is the electron band gap in the absence of the electric field [77-78]; $n_a = 2 \cdot 10^{28}$ m$^{-3}$ is the saturation density [75]; $I = \frac{n}{2}\sqrt{\frac{\varepsilon_0}{\mu_0}}\left|\vec{E}\right|^2$ - intensity; $n = 1.45$ [67] is the refractive index of unexcited fused silica for laser wavelength $\lambda = 800$ nm.

### 2.2 Electron density evolution

To account the transient changes in material characteristics due to nonlinear processes taking place during high-intensity ultrafast laser irradiation, Maxwell's equations are coupled with the rate equation for free carrier number density as follows

$$\frac{\partial n_e}{\partial t} = W_{PI} + W_{av} - \frac{n_e}{\tau_{tr}}, \quad (5)$$

where $W_{PI}$ corresponds to the photoionization effect

$$W_{PI} = (n_a - n_e) w_{pi}, \quad (6)$$

and $\tau_{tr} = 150$ fs is the electron trapping time reported in Ref. [75, 79-81] and commonly used in numerical simulations to describe fast electron trapping at the surface and in fused silica bulk [64, 67, 82-83] .

The avalanche ionization rate is described via the Drude formalism [78]:

$$W_{av} = \frac{e^2 \tau_c n_e \left|\vec{E}^2\right|}{m_e E_g^* (1+\omega^2\tau_c^2)\left[1 + m_e^*/m_e\right]} \cdot \frac{n_a - n_e}{n_a}, \quad (7)$$

where $E_g^* = E_g + e^2\left|\vec{E}^2\right|/4m_e^*\omega^2$ is the effective band gap [77], $m^* = 0.5\ m_e$ [75] is the reduced electron mass.

Note, that in Fig. 1-7 the electron density is normalized to its critical value $n_{cr} = 1.74\cdot10^{27}$ m$^{-3}$ at $\lambda = 800$ nm [67].

In what follows, we focus attention on the investigation of the electronic modification induced by single pulse ultrashort laser irradiation of glass containing randomly distributed inhomogeneities, which are considered to be nanoregions with a narrower electron band gap $E_g = 5.2$ eV [73].

### 2.3 Polarization states

Initial electric field source for linear polarization source is introduced as follows

$$E^{lin}(t,r,z) = \frac{w_0}{w(z)}\exp\left(-\frac{(t-t_0)^2}{\theta^2}\right)\cdot \cdot\exp\left(i\omega t - \frac{r^2}{w^2(z)} - ikz - ik\frac{r^2}{2R(z)} + i\varsigma(z)\right), \quad (8)$$

where $\theta = 120$ fs is the pulse width at half maximum (FWHM), $t_0$ is a time delay, $w_0 = 1.5$ μm is the waist beam, $w(z) = w_0\sqrt{1+\left(\frac{z}{z_R}\right)^2}$ is the Gaussian beam's spot size, $\omega = 2\pi c/\lambda$ is the angular frequency, $\lambda = 800$ nm is the laser wavelength, $z_R = \pi w_0^2 n_0/\lambda$ is the Rayleigh length, $r = \sqrt{x^2+y^2}$ is the radial distance from the beam's waist, $R_z = z\left[1+\left(\frac{z_R}{z}\right)^2\right]$ is the radius of curvature of the wavefront comprising the beam, and $\varsigma(z) = \arctan\left(\frac{z}{z_R}\right)$ is the Gouy phase shift. $z = 0$ corresponds to the position of the beam waist.

For circular polarization, we introduce the initial electric field source as the superposition of two linear polarizations with a phase difference of $\pi/2$

$$\begin{cases} E_x \sim \cos(\omega t - kz) \\ E_y \sim \sin(\omega t - kz). \end{cases} \quad (9)$$

For more complex polarization states, we use the following parametrization

$$\begin{cases} E_x = E^{lin}\left[cos(Arg)e_x - \sin(Arg)e_y\right] \\ E_y = E^{lin}\left[cos(Arg)e_y - \sin(Arg)e_x\right], \end{cases} \quad (10)$$

where $e_x = x/\sqrt{x^2+y^2}$ and $e_y = y/\sqrt{x^2+y^2}$ are the components of the unit vector due to the conversion from cylindrical to Cartesian system of coordinates. Therefore, if $Arg = 0$, the polarization is radial; if $Arg = \pi/2$, it is azimuthal. On the whole, it could be written as $Arg = 2\pi Nr/R_0 - \arcsin(e_y) + \alpha_0$, where the first part stands for radial-variant polarization, the second gives the azimuthal-variant polarization, and $\alpha_0$ is a constant [84]. $N$ is referred to the radial index, which defines the number of maxima/minima, and $R_0$ is the beam radius of radial-variant vector field. The intensity patterns exhibit the extinction rings, implying that the polarization is radial-variant. The number of extinction rings is $2N$, the radius of the $i^{th}$ extinction ring is given by $R_i = (2i-1)R_0/4N$ and the spatial interval between two separate rings $\Delta R = R_0/2N$.

## 3. Results and discussion

### 3.1 Linear polarization state

Fig. 1 shows the electron density profiles calculated by 3D-FDTD coupled with electron density evolution equation (1-7) for linearly polarized beam (8). The light propagates in $z$ direction inside a glass sample with initial bulk nanoroughness. Nanoplasmas elongate from randomly distributed inhomogeneities perpendicular to the light polarization moving by strong near-field enhancement and multiphoton ionization of intensity enhanced regions during ultrashort laser irradiation. Fields interference due to multiple scattering from inhomogeneities leads to sub-wavelength periodicity of the electron density $n_e(x,y,z)$ both in $xOz$ and $xOy$ planes [73]. Fourier Transform (FT) is performed to analyze the results in the frequency domain in Fig. 1(c). In fact, the maximum corresponds to $k_x \sim 3k_0$, which identifies the periodicity of $\lambda/2n$ in fused silica reported in independent experiments [59, 61, 85-87].

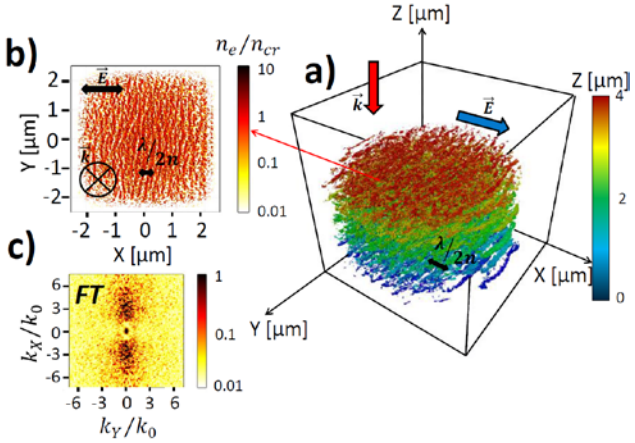


**Fig. 1** Calculation results obtained by linear polarization irradiation. (a) Electron density distribution $n_e > 0.1n_{cr}$ calculated by 3D-FDTD coupled with electron density equation *80* fs after the pulse peak. Pulse duration is *120* fs (FWHM). (b) Cross-section of the electron density, corresponding to $z = 4$ μm. (c) Corresponding Fourier Transform (FT). The pulse energy is fixed to *500* nJ. Laser wavelength $\lambda$ is *800* nm in air. The wave numbers $k_x$ and $k_y$ are normalized to the incident wave number $k_0=2\pi/\lambda$. Initial concentration of randomly distributed inhomogeneities $C_i = 1\%$. Initial size of inhomogeneities $r = 5$ nm.

In fact, the periodicity of the nanostructures depends on the local concentration of inhomogeneities [73], which could be controlled by the number of applied pulses. For example, an increase of the concentration from $C_i = 1\%$ to $C_i = 3\%$ significantly influences the periodicity and the thickness of the self-organized nanogratings in Fig. 2(a). While performing FT, the maximum is displaced closer to $k_x \sim 4.5k_0$, which corresponds to the periodicity of $\lambda/3n$ in fused silica. Therefore, different sub-wavelength periodici-

ties obtained in experiments [11, 88-90] are explained by variable bulk nanoroughness.

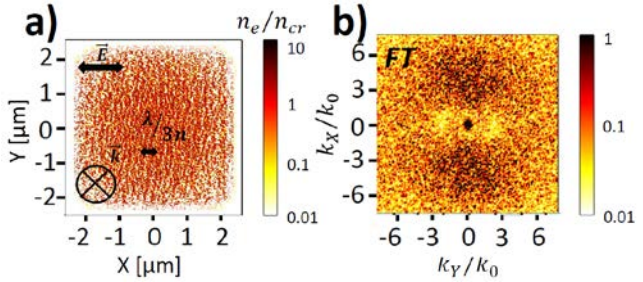


**Fig. 2** (a) Electron density profile calculated by 3D-FDTD coupled with electron density equation *80* fs after the pulse peak. Pulse duration is *120* fs (FWHM). (b) Corresponding Fourier Transform (FT). The pulse energy is fixed to *500* nJ. Laser wavelength $\lambda$ is *800* nm in air. The wave numbers $k_x$ and $k_y$ are normalized to the incident wave number $k_0=2\pi/\lambda$. Initial concentration of randomly distributed inhomogeneities $C_i = 3\%$. Initial size of inhomogeneities $r = 5$ nm.

### 3.2 Azimuthal-variant polarization states

Herein, we present the calculation results for three azimuthal variant polarization sources (10): radial *(Arg = 0)*, azimuthal *(Arg = π/2)*, and spiral *(Arg = π/4)*. Fig. 3 shows that the optical material response is local and the nanostructures orientation is defined by the local electric field polarization. As in the case of linear polarization, nanoplasmas elongate strictly perpendicularly to the laser polarization. Because of azimuthal-variant behavior of the polarization state, the desirable nanostructures orientation could be achieved. Radial polarization beam induces ring-like self-organization in Fig. 3(a, d), whereas the azimuthal polarization beam creates radially oriented nanoplasmas in Fig. 3(b, e). The polarization-dependent azimuthal-variant nanostructuring was reported in numerous experimental works on surface nanostructuring [1-7, 23] and in fused silica bulk [13, 15, 19-20].

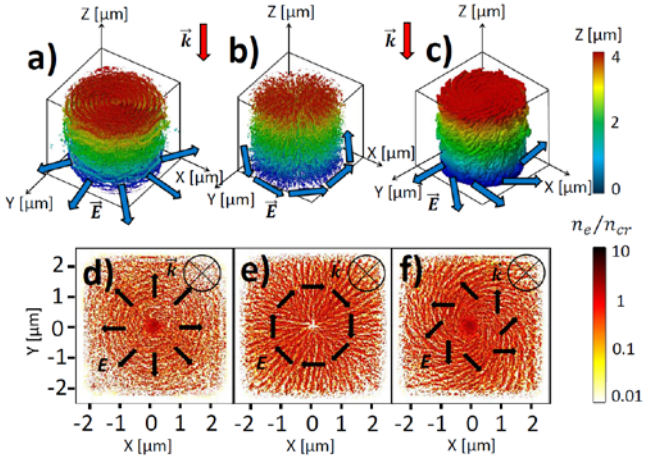


**Fig. 3** Calculated shape of the electronic modification induced by radial (a, d), azimuthal (b, e) and spiral (c, f) polarization irradiation. (a, b, c) - Electron density distribution $n_e > 0.1n_{cr}$ calculated by 3D-FDTD coupled with electron density equation *80* fs after the pulse peak. Pulse duration is *120* fs (FWHM). (d, e, f) - Cross-section of the electron density, corresponding to $z = 4$ μm. The pulse energy is fixed to *1* μJ. Laser wavelength $\lambda$ is *800* nm in air. Initial concentration of randomly distributed inhomogeneities $C_i = 1\%$. Initial size of inhomogeneities $r = 5$ nm.

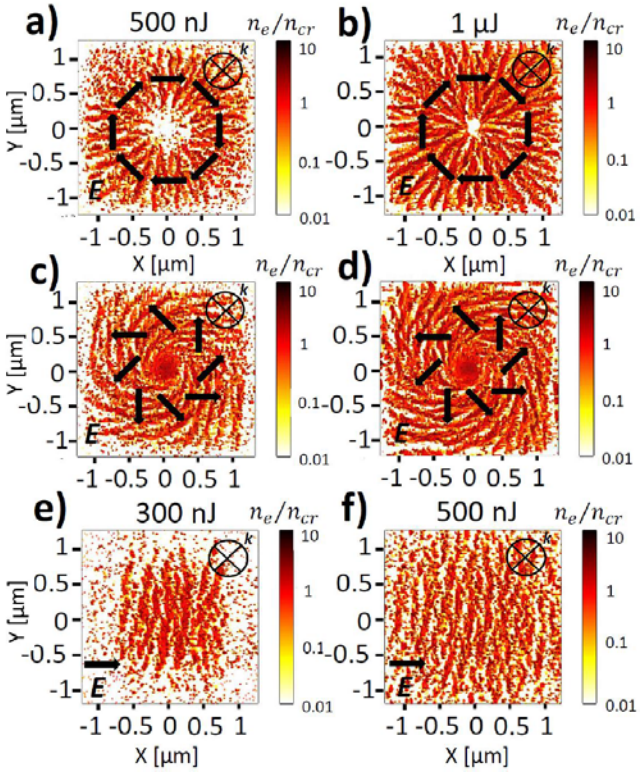


**Fig. 4** Calculated electron density profiles imprinted by azimuthal (a, b), spiral (c, d) and linear (e, f) polarization irradiation *80* fs after the pulse peak. Pulse duration is *120* fs (FWHM). The pulse energies are *300* nJ (e), *500* nJ (a, c, f) and *1* μJ (b, d). Laser wavelength $\lambda$ is *800* nm in air. Initial concentration of randomly distributed inhomogeneities $C_i = 0.5\%$. Initial size of inhomogeneities $r = 5$ nm.

The superposition of radial and azimuthal polarizations leads to self-organization of Archimedian nanospiral structures [4, 7, 23]. The particularity of the nanoscale spiral structures is their unique inversion symmetry with an enhanced spectrally complex optical response, making them a strong candidate for nonlinear optical applications [91-96]. The electron density profile of the corresponding windmill-like modification is shown in Fig. 3(c, f).

In what follows, we analyze the electron density profiles induced by different intensity irradiation with azimuthal-variant and linear polarization states in Fig. 4. On one hand, larger area is covered with high-density plasma and new more pronounced nanostructures are organized at high fluences. On the other hand, the nanogratings period remains unchanged independently of the pulse energy in agreement with Bhardwaj et al. [59]. In fact, similar behavior was revealed experimentally by applying azimuthal and radial polarizations [13]. The period of the self-organized nanostructures was estimated to lie between $\lambda/4n \sim 125$ nm and $\lambda/2n \sim 260$ nm [63].

Note, that no pronounced modification is induced in the center by applying azimuthally polarized beam in Fig. 4(a, b), whereas the electronic densification occurs by using spiral [Fig. 3f, 4(c, d)] and radial polarizations [Fig. 3d, 5a] for the same laser irradiation conditions. Such behavior could be explained by sharp longitudinal electric field

component at the focus and, consequently, larger energy deposition in the center in the case of radial polarization [31, 97]. In contrast, the electric field is purely transverse and zero in the center for azimuthal polarization, therefore, there is no electronic densification. These numerical results are in agreement with the experimentally revealed modifications induced by single pulse irradiation by radially and azimuthally polarized beams [13].

### 3.3 Radial-variant polarization states

Experiments reveal that at certain laser conditions the laser-induced nanostructures tend to self-organize forming nanoplanes perpendicular to the local laser irradiation in fused silica [11-15]. Despite the ability to control the nanostructures characteristics by changing the laser parameters [12-15, 61, 74], both the spatial configuration and the uniformity of the nanostructures strongly depend on the pristine glass material and bulk nanoroughness, thus, the process is not always predictable [83, 98]. From the other point of view, the control over the precise configuration could open new opportunities in the laser nanostructuring [23, 41-43].

Previously, it was shown that radially polarized beams and, especially, beams having radial-variant states, were beneficial in nanoscale precise processing such as optical trapping of nanoparticles and plasmon excitation comparing to linearly polarized beams [32-34, 41-47]. In our case, the manipulation over the nanoscale inhomogeneities is based on Mie scattering and multiphoton ionization processes which take place under femtosecond laser irradiation. Therefore, it could be advantageous to have spatial control over the nanoplasmas evolution as well by applying radial-variant polarization beams.

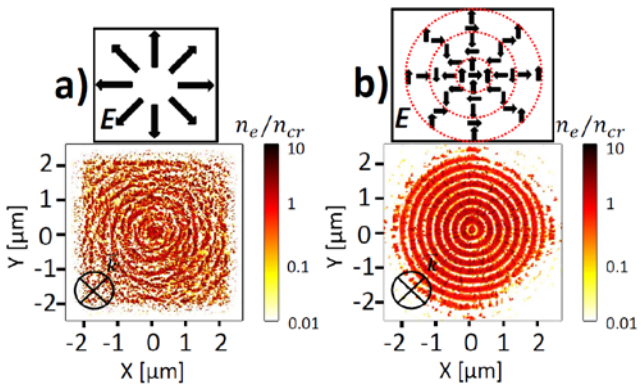


**Fig. 5** Electron density profiles imprinted by radial- (a) and radial-azimuthal-variant (b) polarization irradiation *80* fs after the pulse peak. Pulse duration is *120* fs (FWHM). The pulse energies are *500* nJ (a) and 2 μJ (b). Laser wavelength $\lambda$ is *800* nm in air. Initial concentration of randomly distributed inhomogeneities $C_i = 0.5\%$. In the case of radial-variant state (b), the beam radius is fixed to be $R_0 = 1$ μm and $N = 2$, resulting in $\Delta R = 250$ nm periodicity. Initial size of inhomogeneities $r = 5$ nm.

Nanoplasmas, which evolve into self-organized patterns from randomly distributed inhomogeneities, elongate during ultrashort laser irradiation in one underlined direction perpendicular to the local laser irradiation. In the case of radial-variant polarization, the local laser polarization changes from radial to azimuthal periodically along the radial direction. Local radial polarization provides strong longitudinal electric field force contributing to the formation of periodical rings, whereas local azimuthal polarization results in the local intensity enhancement along the radial direction, which defines the thickness of the ring-shape modification. Therefore, the mechanism of the electron densification in the case of the radial-variant polarization is the same as by using radial polarization. However, if in the case of radial polarization the process of self-organization and the final periodicity of the nanostructures were attributed to multiple scattering from inhomogenities, whereas it is the consequence of the initial periodic intensity distribution in the case of radial-variant polarization.

An interesting point concerning radial-azimuthal-variant polarization is that the spatial distribution is dependent on the radial vector only while it remains independent of the azimuthal angle [84]. Fig. 5 shows electronic modifications induced by radial polarization with $Arg = 0$ and radial-azimuthal-variant polarization with $Arg = 2\pi Nr/R_0 - \arcsin(e_y)$ (10) in glass with the same bulk nanoroughness. In the first case, shown in Fig. 5(a), the self-organization is uncontrollable, only defined by near-field interaction of laser-induced inhomogeneities and preferred direction of their elongation perpendicular to the local laser polarization. In the second case, as shown in Fig. 5(b), the growth of the nanoplasmas is, however, limited by the regions of the periodic enhanced intensity. The interplay between the self-organization phenomena and the polarization geometry of the beam leads to the structures with well-defined positions and controllable thickness.

### 3.4 Circular polarization state

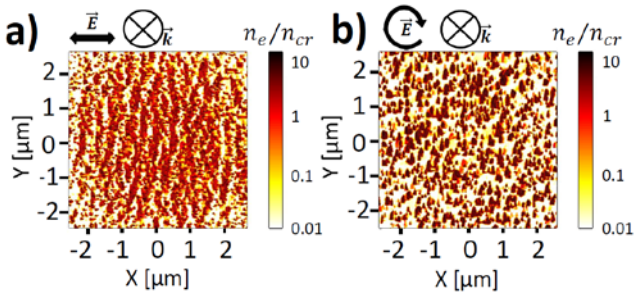


**Fig. 6** Electron density profiles imprinted by linear (a) and circular (b) polarization irradiation *20* fs after the pulse peak. Pulse duration is *120* fs (FWHM). The pulse energy is fixed to *500* nJ. Laser wavelength $\lambda$ is *800* nm in air. Initial concentration of randomly distributed inhomogeneities $C_i = 0.5\%$. Initial size of inhomogeneities $r = 5$ nm.

In what follows, we analyze the electronic modification induced by circularly polarized beam irradiation. The particularity of the circular polarization is that there is no preferred direction in the plane *x0y* because the electric fields $E_x$ and $E_y$ have equivalent contributions (9). In this case, the nanoplasmas from laser-induced inhomogeneities transform into random voxel nanoscale modifications [54]. Fig. 6 compares laser-induced electronic modification by linearly and circularly polarized beams. In the first case, nanoplasmas are stretched perpendicularly to the laser polarization direction, whereas in the second case there is no periodic organization and the laser-modified area is covered by

randomly distributed nanodots resulting from the laser-induced inhomogeneities evolution. Random voxel nanoscale modifications formed after circularly polarized beam irradiation were reported in several experimental works [49-54].

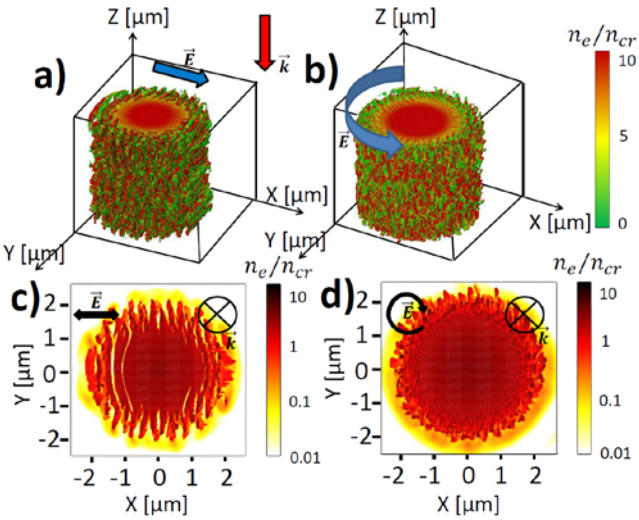


**Fig. 7** Calculated shape of the electronic modification induced by linear and circular polarization irradiation. (a, b) Electron density distribution calculated by 3D-FDTD coupled with electron density equation *80* fs after the pulse peak. Pulse duration is *120* fs (FWHM). (b, d) Cross-section of the electron density, corresponding to $z = 4$ μm. (a, c) correspond to linear polarization, (b, d) to circular polarization. The pulse energy is fixed to *2* μJ. Laser wavelength $\lambda$ is *800* nm in air. Initial concentration of randomly distributed inhomogeneities $C_i = 1\%$. Initial size of inhomogeneities $r = 5$ nm.

Finally, we perform calculations for increased laser beam energy and compare the resulting electronic modifications induced by linear and circular beam irradiation. Fig. 7 shows the electron density distribution after ultrashort laser irradiation by high-intensity linear and circular beams. At the center of the beam focus, high electron densities above the critical value lead to smooth electron density profile. However, laser-induced inhomogeneities contribute to the inhomogeneous energy deposition at the edges of the electronic modification. In the case of linear polarization, the modification is asymmetrical. The nanogratings elongate from the center oriented perpendicular to the laser polarization. In contrast, the electron density distribution induced by circularly polarized beam is quasi-symmetrical, even in the presence of bulk nanoroughness which results in a propeller-like density profile on the interface of the electronic modification.

In summary, laser processing with circular beam is advantageous in the case we desire avoid distortions.

The results of numerical calculations demonstrate the electronic modification of the material, which is believed to result in a further permanent modification in the form of nanogratings. A more complex separate multi-physical investigation, including two-temperature model, a system of thermoelastic wave equations and equations of state, is required to analyze the thermomechanical evolution of nanotransformation in dielectric materials between two femtosecond pulses and to relate the criterion of permanent modification to the criterion of electronic modification. This work is underway and will be presented elsewhere.

## 4. Conclusion

In the presented study, we have discussed the particularities of 3D electron density profiles imprinted by ultrafast laser irradiation of glass with developed bulk nanoroughness. By applying different polarization states, we have demonstrated numerically that the nanostructure orientation is perpendicular to the local laser polarization. The larger bulk nanoroughness leads to a decrease of the nanostructure periodicity, however, to more dispersed and less pronounced structures, while the laser fluence defines the area covered with the nanostructures.

Radially polarized beam is shown to induce ring-like electronic modification with a densification in the center, whereas azimuthally polarized beam creates radially oriented nanoplasmas elongated from the center, where no electronic modification occurs. In the case of windmill polarization, numerical results demonstrate the self-organization of Archimedian spiral nanostructures. Between the combinations of radial and azimuthal polarization states, arbitrary polarized laser beams might be advantageous to allow better control over the nanostructure characteristics. Circular polarization is, however, shown to be beneficial to prevent the nanostructures self-organization, inducing random nanodots at moderate intensities and quasi-symmetrical circular-shaped modification in the case of high-intensity irradiation.

The gained better understanding of the mechanism of nanostructure self-organization opens a wide range of applications in complex security marking, information encoding, creation of photonic components via femtosecond inscription, and data storage [28]. In addition, our results pave the way to deterministic tuning of electron density distributions, defining the final structured organization as a function of the targeted applications.

**Acknowledgments**

This work was supported by the NANODIELEC project, LABEX MANUTECH SISE (ANR-10-LABEX-0075) of Université de Lyon, within the program "Investissements d'Avenir" (ANR-11-IDEX-0007) operated by the French National Research Agency (ANR).

**References**

[1] O. J. Allegre, W. Perrie, S. P. Edwardson, G. Dearden, and K. G. Watkins: J. Opt., 14, (2012) 085601.

[2] K. K. Anoop, R. Fittipaldi, A. Rubano, X. Wang, D. Paparo, A. Vecchione, L. Marrucci, R. Bruzzese, and S. Amoruso: J. Appl. Phys., 116, (2014) 113102.

[3] G. D. Tsibidis, E. Skoulas, and E. Stratakis: Opt. Lett., 40, (2015) 5172.

[4] J. Ouyang, W. Perrie, O. J. Allegre, T. Heil, Y. Jin, E. Fearon, D. Eckford, S. P. Edwardson, and G. Dearden: Opt. Express, 23, (2015) 12562.

[5] W. Shen, C. Cheng, M. Yang, Y. Kozawa, and S. Sato: J. Laser Micro Nanoeng., 5, (2010) 229.

[6] K. Lou, S.-X. Qian, X.-L. Wang, Y. Li, B. Gu, C. Tu, and H.-T. Wang: Opt. Express, 20, (2012) 120.

[7] J. Nivas, S. He, A. Rubano, A. Vecchione, D. Paparo, L. Marrucci, R. Bruzzese, and S. Amoruso: Scientific Reports, 5, (2015) 1.
[8] S. Juodkazis, K. Nishimura, H. Misawa: Appl. Surf. Sci., 253, (2007) 6539.
[9] F. Liang, R. Vallée, and S. L. Chin: Opt. Mat. Express, 2 (2012) 900.
[10] S. Höhm, M. Herzlieb, A. Rosenfeld, J. Krüger, and J. Bonse: Appl. Surf. Sci., 336, (2015) 39.
[11] Y. Shimotsuma, P. G. Kazansky, J. Qiu, and K. Hirao: Phys. Rev. Lett., 91, (2003) 247405.
[12] C. Hnatovsky, R. S. Taylor, E. Simova, P. P. Rajeev, D. M. Rayner, V. R. Bhardwaj, and P. B. Corkum: Appl. Phys. A, 84, (2006) 47.
[13] C. Hnatovsky, V. Shvedov, W. Krolikowski, and A. Rode: Phys. Rev. Lett., 106, (2011) 123901.
[14] Y. Dai, G. Wu, X. Lin, G. Ma, and J. Qiu: Opt. Express, 20, (2012) 18072.
[15] R. Stoian, K. Mishchik, G. Cheng, C. Mauclair, C. D'Amico, J. P. Colombier, and M. Zamfirescu: Opt. Mat. Express, 3, (2013) 1755.
[16] T. Okada, T. Tomita, S. Matsuo, S. Hashimoto, Y. Ishida, S. Kiyama, and T. Takahashi: J. Appl. Phys., 106, (2009) 054307.
[17] M. Mori, Y. Shimotsuma, T. Sei, M. Sakakura, K. Miura, and H. Udono: Phys. Status Solidi A, 212, (2015) 1.
[18] Y. Shimotsuma, T. Sei, M. Mori, M. Sakakura, and K. Miura, Appl. Phys. A, 122, (2016) 1.
[19] C. Hnatovsky, V. Shvedov, W. Krolikowski: Opt. Express, 21, (2013) 12651.
[20] B. McMillen, and Y. Bellouard: Opt. Express, 23, (2015) 86.
[21] R. S. Taylor, E. Simova, and C. Hnatovsky: Opt. Lett., 33, (2008) 1312.
[22] J.-T. Chen, W.-C. Lai, Y.-J. Kao, Y.-Y. Yang, and J.-K. Sheu: Opt. Express, 20, (2012) 5689.
[23] S. Hasegawa, and Y. Hayasaki: Int. Journal of Optomechatronics, 8, (2014) 73.
[24] Y. Shimotsuma, M. Sakakura, P. G. Kazansky, M. Beresna, J. Qiu, K. Miura, and K. Hirao: Advanced Materials, 22, (2010) 4039.
[25] M. Beresna, M. Gecevicius, and P. G. Kazansky: Opt. Mater. Express, 1, (2011) 783.
[26] W. Cai, A. R. Libertun, and R. Piestun: Opt. Express, 14, (2006) 3785.
[27] M. Beresna, M. Gecevicius, P. G. Kazansky, and T. Gertus: Appl. Phys. Lett., 98, (2011) 201101.
[28] Y. Jin, O. J. Allegre, W. Perrie, K. Abrams, J. Ouyang, E. Fearon, S. P. Edwardson, and G. Dearden: Opt. Express, 21, (2013) 25333.
[29] Y. Liao, Y. Cheng, C. Liu, J. Song, F. He, Y. Shen, D. Chen, Z. Xu, Z. Fan, X. Wei, K. Sugioka, and K. Midorikawa: Lab on a Chip, 13, (2013) 1626.
[30] O. J. Allegre, Y. Jin, W. Perrie, J. Ouyang, E. Fearon, S. P. Edwardson, and G. Dearden: Opt. Express, 21, (2013) 21198.
[31] R. Dorn, S. Quabis, and G. Leuchs: Phys. Rev. Lett., 91, (2003) 233901.
[32] P. S. Tan, X.-C. Yuan, J. Lin, Q. Wang, and R. E. Burge: Opt. Express, 16, (2008) 18451.
[33] Z. J. Hu, P. S. Tan, S. Zhu, and X.-C. Yuan: Opt. Express, 18, (2010) 10864.
[34] G. H. Yuan, X.-C. Yuan, J. Bu, P. S. Tan, and Q. Wang: Opt. Express, 19, (2011) 224.
[35] M. Dienerowitz, M. Mazilu, P. J. Reece, T. F. Krauss, and K. Dholakia: Opt. Express, 16, (2008) 4991.
[36] M. A. Tyrk, S. A. Zolotovskaya, W. A. Gillespie, and A. Abdolvand: Opt. Express, 23, (2015) 23394.
[37] G. Rui, X. Wang, and Y. Cui: Opt. Express, 23, (2015) 25707.
[38] S. Roy, K. Ushakova, Q. Van den Berg, S. F. Pereira, and H. P. Urbach: Phys. Rev. Lett., 114, (2015), 103903.
[39] M. Suzuki, K. Yamane, K. Oka, Y. Toda, and R. Morita: Scientific Reports, 5, (2015) 1.
[40] V. Parigi, V. D'Ambrosio, C. Arnold, L. Marrucci, F. Sciarrino, and J. Laurat: Nat. Commun., 6, (2015) 1.
[41] K. Lou, S.-X. Qian, Z.-C. Ren, C. Tu, Y. Li, and H.-T. Wang: Scientific Reports, 3, (2013) 1.
[42] S. Hasegawa, and Y. Hayasaki: Opt. Express, 21, (2013) 12987.
[43] M.-Q. Cai, P.-P. Li, D. Feng, Y. Pan, S.-X. Qian, Y. Li, C. Tu, and H.-T. Wang: Opt. Express, 41, (2016) 1474.
[44] X.-L. Wang, J. Ding, W.-J. Ni, C.-S. Guo, and H.-T. Wang: Opt. Lett., 32, (2007) 3549.
[45] X.-L. Wang, Y. Li, J. Chen, C.-S. Guo, J. Ding, and H.-T. Wang: Opt. Lett., 18, (2010) 10786.
[46] Z.-Y. Rong, Y.-J. Han, S.-Z. Wang, and C. S. Guo: Opt. Express, 22, (2014) 1636.
[47] R.-P. Chen, Z. Chen, K.-H. Chew, P.-G. Li, Z. Yu, J. Ding, and S. He: Scientific Reports, 5, (2015) 1.
[48] K. Cvecek, I. Alexeev, I. Miyamoto, and M. Schmidt: Physics Procedia, 5, (2010) 495.
[49] N. Yasumaru, K. Miyazaki, and J. Kiuchi: Appl. Phys. A, 76, (2003) 983.
[50] O. Varlamova, J. Reif, S. Varlamov, and M. Bestehorn: Appl. Surf. Sci., 257, (2011) 5465.
[51] G. Miyaji, and K. Miyazaki: Opt. Express, 16, (2008) 16265.
[52] R. A. Ganeev, M. Baba, T. Ozaki, and H. Kuroda: J. Opt. Soc. Am. B, 27, (2010) 1077.
[53] J. Reif, F. Costache, O. Varlamova, G. Jia, and M. Ratzke: Phys. Status Solidi C, 6(3), (2009) 681.
[54] K. Mishchik, G. Cheng, G. Huo, I. M. Burakov, C. Mauclair, A. Mermillod-Blondin, A. Rosenfeld, Y. Ouerdane, A. Boukenter, O. Parriaux, and R. Stoian: Opt. Express, 18, (2010) 24809.
[55] G. Fibich, and B. Ilan: Phys. Rev. E, 67, (2003) 036622.
[56] L. Ye, W. Perrie, O. J. Allegre, Y. Jin, Z. Kuang, P. J. Scully, E. Fearon, D. Eckford, S. P. Edwardson, and G. Dearden: Laser. Phys., 23, (2013) 126004.
[57] H. Zhang, M. Tang, J. McCoy, and T.-H. Her: Opt. Express, 15, (2007) 5937.
[58] R. Sugawara, S. Sekiguchi, and T. Yagi: Appl. Surf. Sci., 353, (2015) 400.
[59] V. R. Bhardwaj, E. Simova, P. P. Rajeev, C. Hnatovsky, R. S. Taylor, D. M. Rayner, and P. B. Corkum: Phys. Rev. Lett., 96, (2006) 057404.
[60] G. Cheng, K. Mishchik, C. Mauclair, E. Audouard, and R. Stoian: Opt. Express, 17, (2009) 9515.

[61] R. S. Taylor, C. Hnatovsky, and E. Simova: Laser & Photonics Review, 2, (2008) 26.
[62] J. Z. P. Skolski, G. R. B. E. Römer, J. V. Obona, V. Ocelik, A. J. Huis in 't Veld, and J. Th. M. De Hosson: Phys. Rev. B, 85, (2012) 075320.
[63] V. Makin, and R. Makin: Optics and Spectroscopy, 115, (2013) 591.
[64] R. Buschlinger, S. Nolte, and U. Peschel: Phys. Rev. B, 89, (2014) 184306.
[65] B. Poumellec, M. Lancry, R. Desmarchelier, E. Hervé, F. Brisset, and J. C. Poulin: Opt. Mat. Express, 3, (2013) 1586.
[66] J. Reif, O. Varlamova, S. Uhlig, S. Varlamov, and M. Bestehorn: Appl. Phys. A, 117, (2014) 179.
[67] N. M. Bulgakova, V. P. Zhukov, and Y. P. Meshcheryakov: Appl. Phys. B, 113, (2013) 437.
[68] T.-H. Her: "Comprehensive nanoscience technology" ed. by G. Scholes and G. Wiederrecht, (Elsevier, 2011) p.277-314.
[69] J. Z. P. Skolski, G. R. B. E. Römer, J. V. Obona, and A. J. Huis in 't Veld: J. Appl. Phys., 115, (2014) 103102.
[70] J.-L. Déziel, J. Dumont, D. Gagnon, L. J. Doubé, S. H. Messaddeq, and Y. Messaddeq: J. Opt., 17, (2015) 075405.
[71] H. Zhang, J.-P. Colombier, C. Li, N. Faure, G. Cheng, and R. Stoian: Phys. Rev. B, 92, (2015) 174109.
[72] J.-L. Déziel, J. Dumont, D. Gagnon, and L. J. Dubé: Phys. Status Solidi (c), 13, (2016) 121.
[73] A. Rudenko, J.-P. Colombier, and T. E. Itina: Phys. Rev. B, 93, (2016) 075427.
[74] P. K. Velpula, M. K. Bhuyan, F. Courvoisier, H. Zhang, J.-P. Colombier, and R. Stoian: Laser & Photonics Reviews, 10(2), (2016) 230.
[75] P. Martin, S. Guizard, P. Daguzan, G. Petite, P. D'Oliveira, P. Meynadier, and M. Perdrix: Phys. Rev. B, 55, (1997) 5799.
[76] L. V. Keldysh: Sov. Phys. JETP, 20, (1965) 1307.
[77] B. Rethfeld: Phys. Rev. Lett., 92, (2004) 187401.
[78] X. Jing, J. Shao, J. Zhang, Y. Jin, H. He, and Z. Fan: Opt. Express, 17(26), (2009) 24137.
[79] P. Audebert, Ph. Daguzan, A. Dos Santos, J. C. Gauthier, J. P. Geindre, S. Guizard, G. Hamoniaux, K. Krastev, P. Martin, G. Petite, and A. Antonetti: Phys. Rev. Lett., 73, (1994) 1990.
[80] Q. Sun, H.-B. Jiang, Y. Liu, Y.-H. Zhou, H. Yang, Q.-H. Gong: Chin. Phys. Lett., 23, (2006) 189.
[81] D. Grojo, M. Gertsvolf, S. Lei, T. Barillot, D. M. Rayner, and P. B. Corkum: Phys. Rev. B, 81, (2010) 212301.
[82] A. Couairon, L. Sudrie, M. Franco, B. Prade, and A. Mysyrowicz: Phys. Rev. B, 71, (2005) 125435.
[83] B. Rethfeld, O. Brenk, N. Medvedev, H. Krutsch, D. H. H. Hoffmann: Appl. Phys. A, 101, (2010) 19.
[84] H.-T. Wang: "Vectorial Optical Fields: Fundamentals and Applications" ed. by Q. Zhang, (World Scientific Publishing, 2014) p.27-45.
[85] M. Hörstmann-Jungemann, J. Gottmann, and D. Wortmann: JLMN, 4(2), (2009) 135.
[86] Q. Zhang, H. Lin, B. Jia, L. Xu, and M. Gu: Opt. Express, 18(7), (2010) 6885.
[87] M. Lancry, F. Zimmerman, R. Desmarchelier, J. Tian, F. Brisset, S. Nolte, and B. Poumellec: Appl. Phys. B, 122, (2016) 1.
[88] Y. Liao, W. Pan, Y. Cui, L. Qiao, Y. Bellouard, K. Sugioka, and Y. Cheng: Optics Letters, 40(15), (2015) 3623.
[89] S. Richter, M. Henrich, S. Döring, A. Tünnermann, S. Nolte, and U. Peschel: Journal of Laser Applications, 24, (2012) 042008.
[90] Md. S. Ahsan, M. S. Lee, M. K. Hasan, Y.-C. Noh, I.-B. Sohn, F. Ahmed, and M. B. G. Jun: Optik, 126(24), (2015) 5979.
[91] T. Ohno, and S. Miyanishi: Opt. Express, 14, (2006) 6285.
[92] J. I. Ziegler, and R. F. Haglund: Nano Lett., 10, (2010) 3013.
[93] F. Intonti, N. Caselli, N. Lawrence, J. Trevino, D. S. Wiersma, and L. Dal Negro: New Journal of Physics, 15, (2013) 085023.
[94] J. Lie, C. Yang, H. Zhao, F. Lin, and X. Zhu: Opt. Express, 22, (2014) 16687.
[95] W.-Y. Tsai, J.-S. Huang, and C. B. Huang: Nano Lett., 14, (2014) 547.
[96] R. B. Davidson, J. I. Ziegler, G. Vargas, S. M. Avanesyan, Y. Gong, W. Hess, and R. F. Haglund: Nanophotonics, 4, (2015) 108.
[97] K. S. Youngworth and T. G. Brown: Optics Express, 7, (2000) 77.
[98] N. Groothoff, M.-O. Hongler, P. G. Kazansky, and Y. Bellouard: Opt. Express, 23, (2015) 16993.

(Received: May 19, 2016, Accepted: August 9, 2016)